Preliminary experiment of fluorescent X-ray computed tomography to detect dual agents for biological study

Quanwen Yu,[a,b] Tohoru Takeda,[a]* Tetsuya Yuasa,[b] Yasuhiro Hasegawa,[b] Jin Wu,[a] Thet-Thet-Lwin,[a] Kazuyuki Hyodo,[c] F. Avraham Dilmanian,[d] Yuji Itai[a] and Takao Akatsuka[b]

[a]Institute of Clinical Medicine, University of Tsukuba, Tsukuba, Ibaraki 305-8575, Japan, [b]Faculty of Engineering, Yamagata University, Yonezawa, Yamagata 992-8510, Japan, [c]Materials Structure Science, High Energy Accelerator Research Organization, Tsukuba, Ibaraki 305, Japan, and [d]Medical Department, Brookhaven National Laboratory, Upton, NY 11973, USA. E-mail: ttakeda@md.tsukuba.ac.jp

The simultaneous observation of various information, such as blood flow, tissue metabolism and distribution of receptors, is quite important in order to understand the functional state of biomedical objects. The simultaneous detectability of contrast agents by fluorescent X-ray computed tomography (FXCT) with synchrotron radiation is examined in this study. The system consisted of a silicon (111) double-crystal monochromator, an X-ray slit system, a scanning table, a PIN diode, a highly purified germanium detector and an X-ray charge-coupled device (CCD) camera. The monochromatic X-ray beam energy was adjusted to 37.0 keV and collimated into a pencil beam of 1 × 1 mm. The fluorescent spectra of the $K\alpha$ lines for iodine and xenon were detected simultaneously. FXCT could image the distribution of both iodine and xenon agents in a phantom clearly and the contrast ratio was significantly better than that of transmission X-ray computed tomography images.

Keywords: fluorescent X-rays; computed tomography; iodine; xenon; multi-agents simultaneous detection.

1. Introduction

In order to detect very low contents of nonradioactive specific materials without making slices of samples, fluorescent X-ray tomography (Cesareo & Mascarenhas, 1989; Takeda *et al.*, 1995; Takeda, Maeda *et al.*, 1996) and fluorescent X-ray computed tomography (FXCT) (Boisseau & Grodzins, 1987; Takeda, Akiba *et al.*, 1996; Takeda *et al.*, 1997, 1998, 1999) are being developed. The basic theoretical consideration of FXCT was presented by Hogan *et al.* (1991) and practical reconstruction methods of FXCT have been applied recently (Yuasa *et al.*, 1997*a*; Rust & Weigelt, 1998). Using FXCT with synchrotron radiation, iodine contrast material filled in a phantom was clearly imaged (Takeda, Akiba *et al.*, 1996; Takeda *et al.*, 1997) as a result of the linear-polarized nature of synchrotron radiation (Iida & Gohshi, 1991). So, for living objects, FXCT is considered as an alternative approach to radioactive examinations with single photon emission computed tomography (SPECT). Thus there are two perspectives for the application of FXCT with synchrotron radiation, *i.e.* the imaging of living objects (Takeda, Akiba *et al.*, 1996; Takeda *et al.*, 1997; Akiba *et al.*, 1997) and the micro-imaging of pathological objects (Takeda *et al.*, 2000, 2001) and materials (Simionovici *et al.*, 1999; Vincze *et al.*, 1999).

In biomedical studies, various kinds of radionuclide agent are used to gather information about an organ, such as blood flow, ischemic state, drug distribution, metabolism, receptor function and apotosis. For example, cerebral blood flow and the density of cerebral cells can be evaluated quantitatively by using radioactive Xe-133 gas and I-123 Iomazenil (ethyl 5,6-dihydro-7-iodo-5-methyl-6-oxo-4*H*-imidazo[1,5-*a*][1,4]benzodiazepine-3-carboxylate), respectively. However, each type of information is usually obtained by a separate examination. In FXCT, images can be obtained from one examination by selecting the fluorescent $K\alpha$ line of the elements, so that the simultaneous detection of multi-agents is possible. In this paper, the possibility of simultaneous multi-agent detection by FXCT is examined using a phantom filled with nonradioactive xenon gas and iodine solution; the FXCT images are compared with transmission X-ray computer tomography (TXCT) images.

2. Materials and methods

2.1. *Fluorescent X-ray computer tomography system with synchrotron radiation*

The FXCT system was constructed at the bending-magnet beamline of BLNE-5A of the Tristan Accumulation Ring (6.5 GeV, 10–30 mA) of the High Energy Accelerator Research Organization, Tsukuba, Japan. The system consisted of a silicon (111) double-crystal monochromator, an X-ray slit system, a scanning table, a highly purified germanium (HPGe) detector with a parallel collimator, a rotating X-ray shutter, an X-ray CCD camera, a PIN diode, and computer system (Fig. 1). Fluorescent X-rays were detected by the HPGe detector, whereas transmission X-rays were detected by the CCD camera.

2.1.1. *X-ray energy selection and the formation of a pencil beam.* The white X-ray beam was monochromated at 37.0 keV using a silicon double-crystal monochromator. The size of the incident monochromatic X-ray beam was 65 × 3 mm (width and height, respectively). To make a pencil beam, the incident monochromatic X-ray was collimated into a 1.0 × 1.0 mm beam (horizontal and vertical directions, respectively) using a tantalum X-ray slit (Kohzu Ltd, Japan).

2.1.2. *Fluorescent X-ray detector.* The fluorescent X-rays were detected by a highly purified germanium detector (LO-AXTH Series, EG&G Ortec Ltd, USA). It was operated in a photon-counting mode. The energy resolution was about 700 eV with a shaping time of 2 µs at 30 keV. The active area of detection of HPGe was 51.2 mm in diameter. The detected energy spectrum was digitized by a DSPEC spectrum master (EG&G Ortec Ltd, USA).

2.1.3. *Transmission X-ray detector.* The transmission X-ray detector was a fibre-optically interfaced X-ray CCD camera cooled by a Peltier thermoelectric cooling device (238 K) (Princeton Instruments Ltd, USA). The X-ray CCD camera had 1240 × 1024 pixels with a pixel size of 22.5 × 22.5 µm. Data were digitized in a 16-bit analog-to-digital converter (ADC). The dynamic range of this detector was about 60000:1. An X-ray shutter was set in front of the X-ray CCD camera to prevent radiation damage. The CCD camera was driven by a controller (Princeton Instruments ST-138) and the data were read into a personal computer (PC) (Dimension, Dell Ltd, USA). The readout timings of the CCD camera and X-ray shutter were synchronized with the trigger pulses generated by the pulse motor controller.

2.1.4. *PIN diode.* The monochromatic X-ray intensity declined exponentially owing to the decrease of the ring current; hence the change of monochromatic X-ray intensity was measured by a PIN diode operated in the current-integration mode by a picoammeter

(486, Keithley Ltd, USA). The measured data were digitized by a 16-bit ADC (BNC 2090, National Instruments Ltd, USA) and read into a PC (Aptiva, IBM Ltd, USA).

2.1.5. *System control.* In the FXCT system, a PC (Presario 5000, Compaq Ltd, USA) controlled a pulse motor controller (AS-NET3, Sigma Koki Ltd, Japan). The pulse motor controller controlled the translation–rotation table and rotating X-ray shutter. An automated data-collection procedure was developed using *Labview* (National Instruments Ltd, USA).

2.2. *Experimental phantom*

The acrylic phantom was 30 mm in diameter with a 5 mm-diameter hole for the contrast agent in a gas chamber of diameter 25 mm (Fig. 2). The experiments were performed with two different conditions: high and low concentrations of agents. In the first case, the phantom was filled with 2 mg ml^{-1} iodine solution {diastereomeric mixture of *N*,*N*′-bis(2,3-dihydroxypropyl)-5-[(hydroxyacetyl)methylamino]-2,4,6-triiodo-1,3-benzenedicarboxamide, Iomeprol 350, Eisai Co. Ltd, Japan; mass attenuation coefficient of iodine at 37.0 keV = 29.95 cm^2 g^{-1}} and a mixture of about 30% xenon gas (Xenopure, Teisan Co. Ltd, Japan; mass attenuation coefficient of xenon at 37.0 keV = 27.36 cm^2 g^{-1}). The second phantom was filled with 0.25 mg ml^{-1} iodine solution and a mixture of about 2% xenon gas.

2.3. *Image reconstruction*

The TXCT images were reconstructed by using a filtered back-projection method with a Shepp and Logan filter. The distributions of the linear attenuation coefficients of the object at the energies of the incident and fluorescent X-rays were estimated from the TXCT data. The FXCT images were reconstructed by an algebraic equation representing the attenuation process using the least-squares method based on singular value decomposition (Yuasa *et al.*, 1997*a*). The projection data of the fluorescent $K\alpha$ line for iodine and xenon were generated by integrating the measured counts after subtracting the Compton background scattering (Jorch & Campbell, 1977). These projection data were also corrected by normalizing the decrease of X-ray intensity.

2.4. *Experimental conditions*

The photon flux in front of the object was approximately 7×10^7 photons mm^{-2} s^{-1} at a beam current of 30 mA. The distance between the surface of the HPGe detector and the object was 200 mm and the distance between the X-ray CCD camera and the object was 500 mm. In the detecting portion of the HPGe detector, excited fluorescent X-rays were accumulated by the parallel collimator (height × width × length = 1 × 35 × 100 mm). The object was scanned in steps of 1 mm translation and 4.5° rotation over a range of 180° with a beam cross section of 1 × 1 mm. The data-acquisition time, for both fluorescent X-ray data and transmission X-ray data, was 5 s at each scanning point. The whole data-acquisition time for the FXCT measurements was approximately 5 h, with 40 projections and 40 translations.

2.5. *Definition of contrast ratio*

To assess the difference in image quality between FXCT and TXCT, the contrast ratio (CR) was defined by the following equation,

$$\mathrm{CR} = (b - a)/a,$$

where b is the average value in a region with the contrast material, and a is the average value in the background area.

3. Results

The fluorescent X-ray energy spectrum of the phantom is shown in Fig. 3. At each 5 s data acquisition, the $K\alpha$ line both for iodine and for

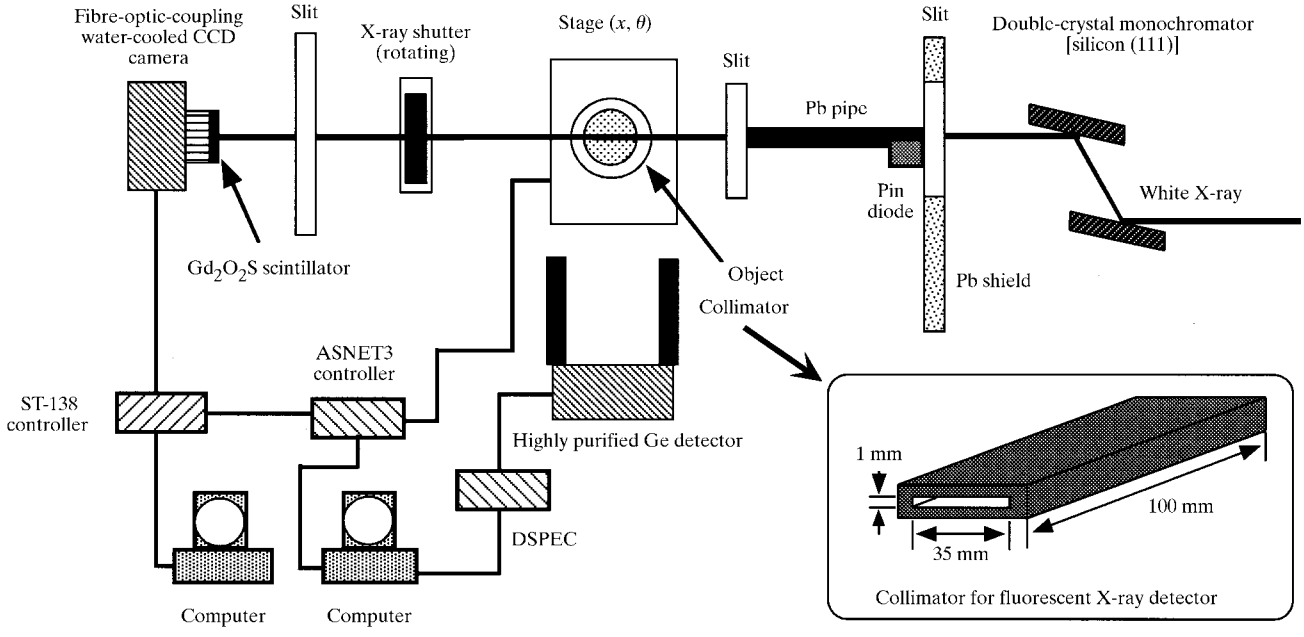

Figure 1
Schematic diagram of the fluorescent X-ray computer tomography system.

Table 1
The fluorescent X-ray counts of FXCT images and the pixel values of TXCT images.

			Background				Background	
	Iodine (2 mg ml^{-1})	Xenon (30%)	Acrylic wall	Air	Iodine (0.25 mg ml^{-1})	Xenon (2%)	Acrylic wall	Air
FXCT	1241 ± 29	864 ± 25	61 ± 4	61 ± 4	125 ± 4	50 ± 2	29 ± 2	29 ± 2
TXCT	227 ± 5	41 ± 4	215 ± 3	35 ± 2	215 ± 5	36 ± 2	215 ± 5	35 ± 2

xenon, and the Compton scattering were detected under both experimental conditions, *i.e.* for high and low concentrations of agents. Using the fluorescent $K\alpha$ line of both iodine and xenon, the distributions of iodine and xenon in the phantom could be imaged separately using just one data acquisition (Figs. 4*a*, 4*b*, 4*d* and 4*e*). In the TXCT image, acrylic phantom structures, the gas chamber filled with 30% xenon gas and the hole filled with 2 mg ml^{-1} iodine solution were represented as regions with different density (Fig. 4*c*). On the other hand, in the TXCT image of 0.25 mg ml^{-1} iodine solution and 2% xenon gas, iodine solution and xenon gas could not be imaged (Fig. 4*f*).

Quantitative analysis was performed for the profiles of the phantom obtained by FXCT and TXCT (Table 1). The values of the contrast ratio (CR) for the FXCT images and for the TXCT image were calculated using the air region as the background. The values of CR for the FXCT images were 19 and 13 in the regions of the 2 mg ml^{-1} iodine solution and the 30% xenon gas, respectively, whereas for the TXCT image the CR values were 0.34 and 0.17, respectively. Hence, the values of CR for the FXCT images were respectively about 56 and 77 times higher than those of the TXCT image. While the CR values were 3.3 and 0.72 in the regions with 0.25 mg ml^{-1} iodine solution and 2% xenon gas, respectively, the contrast was almost zero in the TXCT image.

4. Discussion

4.1. *FXCT performance and its clinical application*

In these preliminary experiments, the fluorescent X-ray spectrum line of two different contrast elements was identified at the excitation energy of 37 keV. By using the fluorescent $K\alpha$ line for iodine and xenon, the distribution of both iodine and xenon were clearly imaged by FXCT; however, the image quality at low concentration decreased slightly because of the small excited fluorescent X-ray count. While the TXCT could image the density changes in the hole and the chamber filled by 2 mg ml^{-1} iodine solution and 30% xenon gas, the contrast elements could not be detected at low concentration. In addition, the discrimination of contrast elements was not possible by TXCT at the single X-ray energy of 37 keV. Quantitative analysis revealed that the sensitivity of FXCT is about 77 times better than that of TXCT.

In a clinical study with single photon emission computed tomography (SPECT), the radioactive agent is used to assess various organic functions, and the content of the radionuclide agent becomes of the order of tens of nanograms per gram (Takeda, Maeda *et al.*, 1996). Since the spatial resolution of SPECT is larger than 7.8 mm (Kouris *et al.*, 1993), the content of the radionuclide agent becomes of the order of tens of nanograms in a voxel of the SPECT image. FXCT can exactly detect 250 ng iodine in a cube of 1 mm^3 (0.25 mg ml^{-1} × 10^{-3} ml), in this experiment, and 200 pg in a cube of 8 × 10^{-3} mm^3, found in a recent experiment (Yu *et al.*, 2000). Thus, FXCT can detect nonradioactive contrast elements at concentrations comparable with those of radioactive agents used in SPECT.

Using the nonradioactive xenon gas with conventional X-ray computer tomography, we can obtain high spatial resolution images, but the concentration of gas must be as high as 30% concentration. The high concentrations of 30% xenon that are inspired cause various side effects, such as discomfort, nausea or headache (Meyer *et al.*, 1988; Richard *et al.*, 1987). In this experiment, the TXCT could not detect 2% xenon gas, whereas, FXCT could image 2% xenon gas because of its high sensitivity. Thus, the concentration of nonradioactive xenon gas can be reduced in FXCT compared with that used in conventional X-ray computer tomography.

In addition, FXCT can use nonradioactive contrast elements other than xenon, so large amounts of elements can be used to obtain

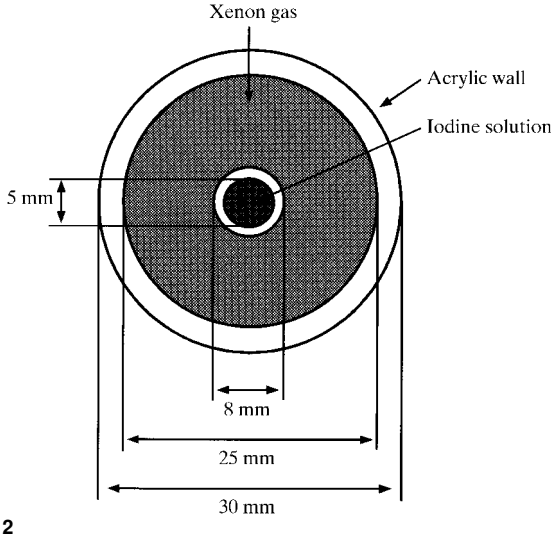

Figure 2
Schematic diagram of the phantom.

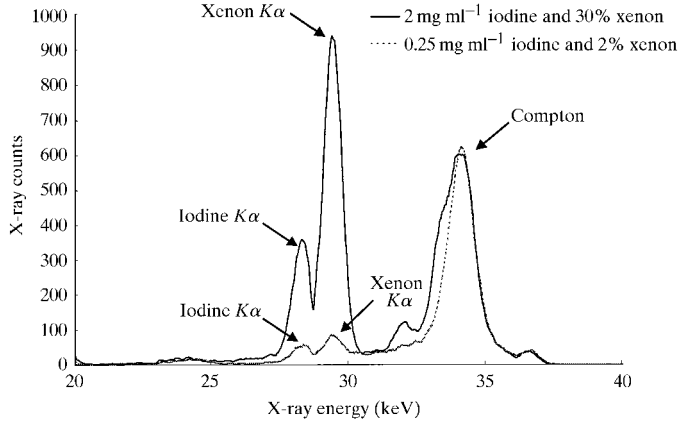

Figure 3
Energy spectrum of the phantom obtained by the fluorescent X-ray computer tomography system.

images with high signal-to-noise ratios, administering more than ten times the dose applied in usual radionuclide examinations and avoiding the significant side effects of drugs.

4.2. *Radiation dose*

For *in vivo* imaging, the radiation dose to the object must be considered. The radiation dose was calculated for a numerical phantom, of 30 mm diameter, filled with water. The absorbed radiation dose D is given by the following equation (Yuasa *et al.*, 1997*b*),

$$D = E_{\rm inc} TR/\rho d^2 h,$$

where the total X-ray absorbed rate, the density of water, the radius of the phantom, the beam height, the energy of the incident beam and the exposure time are R, ρ, d, h, $E_{\rm inc}$ and T, respectively. The absorption dose of the object was 0.39 Gy in this experiment using $R = 9.0 \times 10^9$ photons s^{-1}, $\rho = 1.0 \times 10^{-3}$ g mm^{-3}, $d = 15$ mm, $h = 1$ mm, $E_{\rm inc} = 37.0$ keV and $T = 5$ s.

For the animal experiment, this dose is not significantly higher than that imparted by an X-ray computer tomography study of human (0.2 Gy). However, for clinical study, the dose becomes too high because of the larger object size, so the dose must be reduced by shortening the exposure time, as described in the next section, and/or degrading the spatial resolution by more than 1 mm.

4.3. *Present limitation and future direction*

In these experiments, the distance between the object and the HPGe detector was 200 mm because of the limitation of counting-rate capability and the increment of dead time in the HPGe detector (Yu *et al.*, 2000). The data-acquisition time using fluorescent X-rays was 5 s at each scanning point in order to obtain a sufficient signal-to-noise ratio for the image.

The fluorescent X-ray counts increase geometrically by the inverse square of the distance between the object and the detector. For example, when the distance became 1/4 in the present setup, the fluorescent X-ray counts at the detector increased by 16 times. If a fluorescent detector with high counting-rate capability could be used, the distance between the object and the detector could be shortened and short data-acquisition times would be possible. This also allows the X-ray exposure of the object to be reduced. However, the short distance to the detector causes an increase of background scattered radiation and will decrease the contrast ratio of FXCT images. Thus the estimation model of scattered radiation overlapping the fluorescent $K\alpha$ line must be improved in the near future.

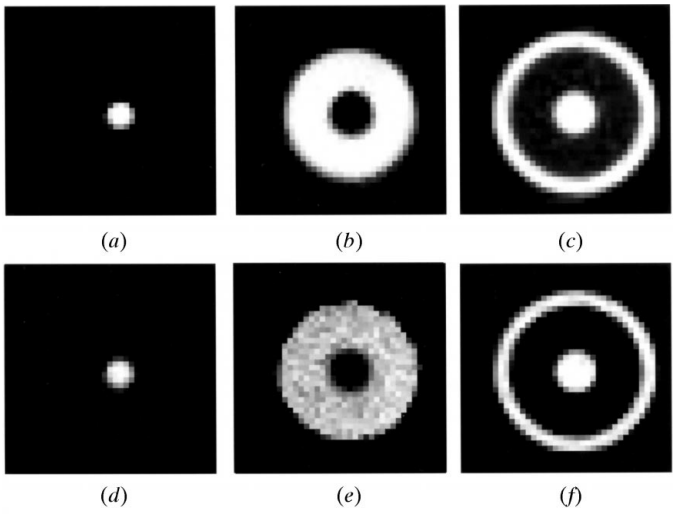

Figure 4
Fluorescent X-ray computer tomography images and transmission X-ray computer tomography images of the phantom. (*a*) FXCT image of 2 mg ml^{-1} iodine solution. (*b*) FXCT image of 30% xenon gas. (*c*) TXCT image of 2 mg ml^{-1} iodine solution and 30% xenon gas. (*d*) FXCT image of 0.25 mg ml^{-1} iodine solution. (*e*) FXCT image of 2% xenon gas. (*f*) TXCT image of 0.25 mg ml^{-1} iodine solution and 2% xenon gas.

5. Conclusions

FXCT generated by the fluorescent $K\alpha$ line can easily distinguish different contrast agents within the object. The phantom study by FXCT demonstrates the high sensitivity of FXCT and the possibility, for biomedical research, of simultaneous imaging in both iodine and xenon at low concentrations.

The authors thank Mr Kouzou Kobayashi for his technical support with the experimental apparatus, and Mrs Yukiko Kawata for her help with the preparation of this paper. This research was supported by a Grant-in-Aid for Science Research #10557084 from the Ministry of Education, Science and Culture. This study was performed under the auspices of the High Energy Accelerator Research Organizations (Proposal No. 99G124). A part of this study was presented at the 6th International Conference on Biophysics and Synchrotron Radiation, held at Argonne, USA, in August 1998 (poster abstracts pp. 34–35).

References

Akiba, M., Takeda, T., Yuasa, T., Uchida, A., Hyodo, K., Akatsuka, T. & Itai, I. (1997). *Med. Elec. Biol. Eng.* **35**, 303–312. (Abstract in English.)
Boisseau, P. & Grodzins, L. (1987). *Hyperfine Interact.* **33**, 283–292.
Cesareo, R. & Mascarenhas, S. (1989). *Nucl. Instrum. Methods A*, **277**, 669–672.
Hogan, J. P., Gonsalves, R. A. & Krieger, A. S. (1991). *IEEE Trans. Nucl. Sci.* **38**, 1721–1727.
Iida, A. & Gohshi, Y. (1991). *Tracer Element Analysis by X-ray Fluorescence*, in *Handbook on Synchrotron Radiation*, Vol. 4, edited by S. Ebashi, M. Koch & E. Rubenstein. Amsterdam: North-Holland, Elsevier.
Jorch, H. H. & Campbell, J. L. (1977). *Nucl. Instrum. Methods.* **143**, 551–559.
Kouris, K., Clarke, G. A., Jarritt, P. H., Townsend, C. E. & Thomas, S. N. (1993). *J. Nucl. Med.* **34**, 1778–1789.
Meyer, J., Shinohara, T., Imai, A., Sakai, M., Hata, T., Oravez, W. T., Timpe, G. M., Deville, T. & Solomon, E. (1988). *Neuroradiology*, **30**, 283–292.
Richard, E. L., Howard, Y., Susan, L. P. & David, G. (1987). *Radiology*, **163**, 251–254.
Rust, G. F. & Weigelt, J. (1998). *IEEE Trans. Nucl. Sci.* **45**, 75–88.
Simionovici, A., Chukalina, M., Drakopoulos, M., Snigireva, I., Snigirev, A., Schroer, C. H., Lengeler, B., Janssens, K. & Adams, F. (1999). *Proc. SPIE*, **3772**, 304–310.
Takeda, T., Akiba, M., Yuasa, T., Kazama, M., Hoshino, A., Watanabe, Y., Hyodo, K., Dilmanian, F. A., Akatsuka, T. & Itai, Y. (1996). *Proc. SPIE*, **2708**, 685–695.
Takeda, T., Itai, Y., Hyodo, K., Ando, M., Akatsuka, T. & Uyama, C. (1998). *J. Synchrotron Rad.* **5**, 326–332.
Takeda, T., Maeda, T., Yuasa, T., Akatsuka, T., Ito, T,. Kishi, K., Wu, J., Kazama, M., Hyodo, K. & Itai, Y. (1995). *Rev. Sci. Instrum.* **66**, 1471–1473.
Takeda, T., Maeda, T., Yuasa, T., Ito, T., Sakamoto, K., Wu, J., Hyodo, K., Dilmanian, F. A., Akatsuka, T. & Itai, Y. (1996). *Med. Imag. Tech.* **14**, 183–194.

Takeda, T., Momose, A., Yu, Q., Yuasa, T., Dilmanian, F. A., Akatsuka, T. & Itai, Y. (2000). *Cell. Mol. Biol.* **46**, 1077–1088.
Takeda, T., Yu, Q., Yashiro, T., Yuasa, T., Hasegawa, Y., Itai, Y. & Akatsuka, T. (1999). *Proc. SPIE*, **3772**, 258–267.
Takeda, T., Yu, Q., Yashiro, T., Zeniya, T., Wu, J., Hasegawa, Y., Thet-Thet-Lwin, Hyodo, K., Yuasa, T., Dilmanian, F. A., Akatsuka, T. & Itai, Y. (2001). *Nucl. Instrum. Methods*. In the press.
Takeda, T., Yuasa, T., Hoshino, A., Akiba, M., Uchida, A., Kazama, M., Hyodo, K., Dilmanian, F. A., Akatsuka, T. & Itai, Y. (1997). *Proc. SPIE*, **3149**, 160–172.
Vincze, L., Janssens, K., Vekemans, B. & Adams, F. (1999). *Proc. SPIE*, **3772**, 328–337.
Yu, Q., Takeda, T., Yashiro, T., Yuasa, T., Hasegawa, Y., Zeniya, T., Hyodo, K., Wu, J., Dilmanian, F. A., Akatsuka, T. & Itai, Y. (2000). *Med. Imag. Tech.* **18**, 805–816.
Yuasa, T., Akiba, M., Takeda, T., Kazama, M., Hoshino, A., Watanabe, Y., Hyodo, K., Dilmanian, F. A., Akatsuka, T. & Itai, Y. (1997*a*). *IEEE Trans. Nucl. Sci.* **44**, 54–62.
Yuasa, T., Akiba M., Takeda,T., Kazama, M., Hoshino, A., Watanabe, Y., Hyodo, K., Dilmanian, F. A., Akatsuka, T. & Itai, Y. (1997*b*). *IEEE Trans. Nucl. Sci.* **44**, 1760–1769.

 Received 31 October 2000 • Accepted 18 December 2000